



Scholars Research Library

Archives of Applied Science Research, 2017, 9 (1):44-51
(<http://scholarsresearchlibrary.com/archive.html>)



Scholars Research Library
ISSN 0975-508X
CODEN (USA) AASRC9

Calcium Carbonate Nanoparticles Enhanced Electrochemical Sensing of DNA

Siddegowda KS, Mallappa M and Shivaraj Y*

Department of Chemistry, Government Science College, Bengaluru-560001, Karnataka, India

ABSTRACT

Calcium carbonate (CaCO_3) nanoparticles were successfully synthesized using calcium hydroxide ($\text{Ca}(\text{OH})_2$) and carbon dioxide gas by bubbling method. Resulting material characterized by powder X-ray diffraction (PXRD), FT-IR, UV-Visible, EDX and SEM. The crystal size of nanoparticles determined by XRD using Debye Scherer formula. FTIR confirmed the formation of calcite, absorption bands at 719 cm^{-1} , 873 cm^{-1} , 1390 cm^{-1} corresponds to in-plane bending (ν_4), out-of-plane bending (ν_2) and asymmetric stretching (ν_3) modes of carbonate group respectively. Morphology and elemental composition of CaCO_3 NPs determined by SEM and EDX, respectively. The prepared nanoparticle further used for the fabrication of carbon paste electrode to determine the electrochemical oxidation of adenine and guanine residues in Fish sperm DNA. The results indicated that the oxidation enhanced peak currents for adenine and guanine residues of FsDNA, as compared with bare carbon paste electrode (BCPE).

Keywords: Calcium carbonate nanoparticles, Double standard fish sperm DNA (FsDNA), Carbon paste electrode, Direct electrochemistry, Bubbling method.

INTRODUCTION

Calcium carbonate nanoparticles are most abundant commercially available inorganic materials and it plays major role in different fields such as paint, rubber, fiber and plastic etc. CaCO_3 NPs exists in three different polymorphic phases such as calcite, vaterite and aragonite [1]. Spanos et al., have shown that the presence of vaterite and aragonite phase in CaCO_3 NPs are thermodynamically stable, which can be stabilized by kinetically or chemically [2]. Due to high biocompatible properties [3-6], higher density and hardness, aragonite showed key role in the production of different industries. It has been observed that, if the metastable vaterite is kept in its solution form long time, would get changed to calcite [7]. Calcite is most thermodynamically stable [4,8] and most important phase in industrial application. Gorna et. el., reported that the properties of calcium carbonate nanoparticles such as morphology, size, phase and size distribution can be customized depending upon its application areas like paper, food processing and sensor [9].

DNA has been used in different fields [10-12] due to its major role in life science and biological functions [13], importantly its nucleotides and their metabolic products showed much effect on coronary and cerebral circulation, control of blood flow, prevention of cardiac arrhythmias, inhibition of neurotransmitter release and modulation of adenylate cyclase activity [14]. In case of diagnosis of cancer, aids, myocardial cellular energy status, disease progress and therapy responses [15], concentration level of nucleotides and their metabolic products were used as important parameter. Compared to other methods, electrochemical methods are the most useful because of its higher sensitivity, lower detection limit, low cost instrumentation and wide potential range [16].

Direct electrochemistry of DNA at mercury electrode gave deep understanding of DNA [17,18] with mainly focusing on the reduction of DNA over mercury electrode and the interaction between the electrode and denaturated DNA. Poly [Ru(vbpy) $_3^{2+}$] film, SWNTs, fullerene- C_{60} -modified GCE [19-21], CNT ceramic electrode [22], carboxylated CNT modified electrode [23], ionic liquid modified electrode [24], and $\text{Fe}_3\text{O}_4/\text{MWCNT}$ nanocomposite modified GCE [25] have been utilized for the detection of DNA, with resulting the lower potential and increased sensitivity depending on the catalytic activity of modified materials.

As per the literature survey, very limited work was reported for direct electrochemical detection of DNA using nanoparticles as a modifier. In the present work, Calcium Carbonate nanoparticles prepared by the reaction of Calcium

hydroxide and Carbon dioxide gas using bubbling method. Furthermore, synthesized material used to fabricate the electrode to investigate the direct electrochemical behavior of FsDNA. The observed result showed an enhanced peak current due to the CaCO₃- nanoparticles modified CPE (CaCO₃ NPs MCPE).

EXPERIMENTAL

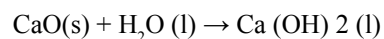
Materials

FsDNA purchased from Sigma-Aldrich. Adenine and guanine purchased from SRL. The supporting electrolyte used for all experiments was 0.1M phosphate buffer solution (PBS) of pH 7, which prepared by the mixture of 0.1M Potassium dihydrogen phosphate and 0.1M Sodium hydroxide solution. All the reagents purchased analytical grade and solutions were prepared from doubly distilled water.

Synthesis of Calcium carbonate nanoparticles

Beaker contains calcium oxide was placed on a water bath with constant temperature (50° C). CO₂ gas bubbler fixed at the bottom of beaker connected with cylinder. As mentioned above, to the prepared slaked solution in a beaker purged with stream of carbon dioxide gas for 1 h under constant stirring of about 300 rpm. The progress of the reaction is monitored by measuring the electrical conductivity and pH of the reaction mixture. When the pH reached below 6.3, indicating the completion of reaction. The resulted suspension is filtered through filter paper, washed with distilled water for several times and dried at 120°C under oven for about 12 h to yield CaCO₃ NPs.

Reaction Mechanism



Preparation of CPE and nanoparticles modified CPE

CaCO₃ NPs MCPE was fabricated by grinding and mixing of 60% graphite powder, 30% nujol oil and 10% CaCO₃ NPs on a mortar to get homogeneous carbon paste. A small portion of CaCO₃ NPs modified Carbon paste filled at one end electrode and the other end connected to electrical circuit through copper wire. CaCO₃ NPs MCPE surface was polished by a piece of tissue paper just before the experiment [26].

Material characterization

Powder XRD data were recorded on Philips X'pert PRO X-ray diffractometer with graphite monochromatized Cu K α radiation ($k=1.541 \text{ \AA}$) in the range of 10°–80° with 2°/min scanning rate. The JEOL-JSM-6490 LV scanning electron microscope with EDS (Kevex Sigma TM Quasar, USA) used to observe the phase structure of CaCO₃ NPs. Fourier transform infrared (FT-IR) spectrum of resulted CaCO₃ NPs was taken by making KBr pellet in Agilent FTIR spectrometer (Australia) over the range of 400-4000 cm⁻¹. Optical property of CaCO₃ NPs studied by UV-Visible absorption spectrophotometer (Shimadzu UV-1800 series). Electrochemical experiments were performed on CH instrument electrochemical analyzer (USA) connected with three-electrode cells as platinum electrode, saturated calomel electrode and carbon paste electrode as counter electrode, reference electrode and working electrode respectively.

RESULTS AND DISCUSSION

Variation of pH and conductivity with time

During the progress of the reaction following observations have been noticed. pH of the solution was changed from 12.79 to 6.24 and conductivity 290 to 33 Siemen/meter, which proved that the formation of CaCO₃ NPs shown in Table 1.

Powder X-ray diffraction study

The phase purity of the CaCO₃ NPs analyzed by powder X-ray diffraction studies. As shown in Figure 1 illustrates that, the peaks with diffraction angle were observed at 23.13°, 29.4°, 31.4°, 36.09°, 39.54°, 43.21°, 47.49°, 48.52°, 56.58°, 57.44°, 60.72°, 64.68° and 72.97° which corresponds to lattice planes (012), (104), (006), (110), (113), (202), (018), (116), (211), (122), (214), (300) and (128) respectively. This data is in good agreement with the JCPDF card no. (5-586) which proves that CaCO₃ NPs is existed in calcite form [27]. The particle size of nanoparticles found to be 38 nm as estimated by relative intensity of peaks and peak sharpness indicates that particles are in crystalline structure.

Table 1: Variation of pH and Conductivity with time

Time (min)	pH	Conductivity (Siemens/metre)
0	12.79	290
1	12.15	230
2	9.6	128
3	6.9	50
4	6.58	41
5	6.36	36
6	6.24	33

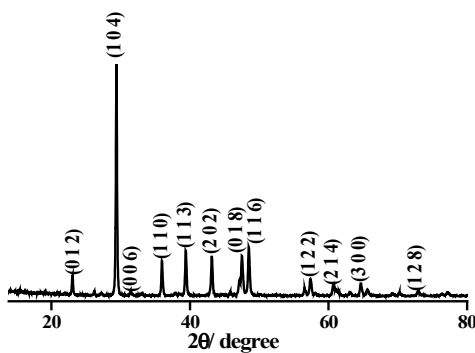


Figure 1: PXRD pattern of CaCO₃ NPs.

The average crystallite size (D) of the nanoparticles calculated by using Debye-Scherer equation [28].

$$D = \frac{k\lambda}{\beta_0 \cos \theta_0}$$

D=shape factor, λ=X-ray wavelength, β=Full width at half maximum of diffraction peak, θ=Bragg angle.

Scanning electron microscope

In order to evaluate the morphology of CaCO₃ NPs, the scanning electron microscope was recorded and shown in Figure 2. The SEM images confirms the nanoparticles are well crystallized with cube/square. CaCO₃ NPs are distributed with agglomeration.

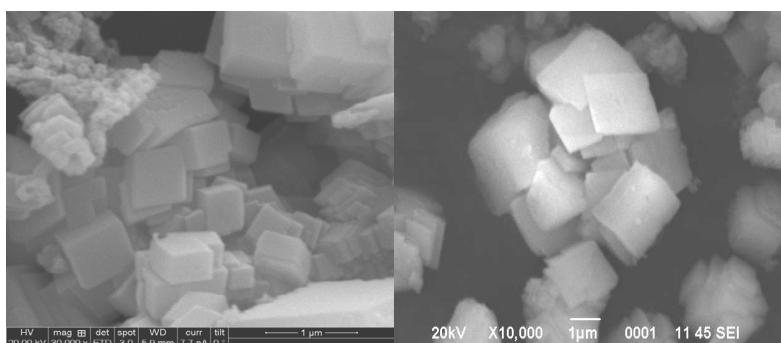


Figure 2: SEM images of CaCO₃ NPs.

Energy dispersive spectroscopy

Elemental analysis of CaCO₃ NPs performed using EDX and shown in Figure 3. The peaks observed at 3.85 keV, 0.5 keV and 0.2 keV corresponds to the binding energies of calcium, oxygen and carbon respectively. Table 2 illustrates the purity of CaCO₃ NPs, expressed in percentage.

Fourier transforms infrared spectroscopy

The structural information of CaCO₃ NPs was determined in the range of 400–2500 cm⁻¹ by using FT–IR spectroscopy. The obtained FT-IR spectrum is as shown in Figure 4. The absorption bands at, 719 cm⁻¹, 873 cm⁻¹, 1390 cm⁻¹

corresponds to in-plane bending (ν_4), out-of-plane bending (ν_2) and asymmetric stretching (ν_3) modes of carbonate group respectively and the peak at 418 cm^{-1} is due to the presence of Ca-O bond. The obtained FT-IR spectra confirmed that, the CaCO_3 NPs showed the characteristic peak of carbonate group.

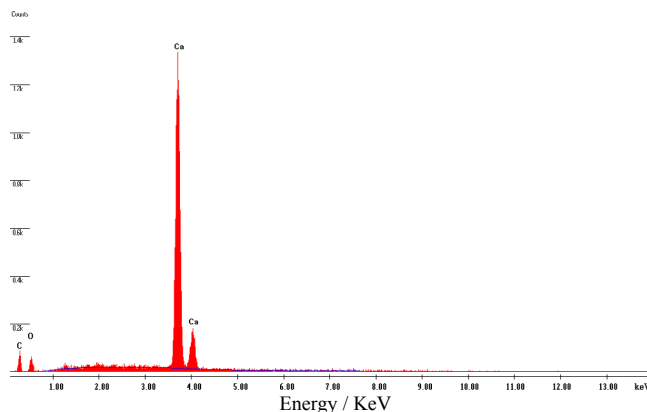


Figure 3: EDX spectrum of CaCO_3 NPs.

Table 2: Percentage of calcium, carbon and oxygen present in CaCO_3 NPs.

Elements	Practical value	Theoretical value
	% (CaCO_3 NPs)	% (1M CaCO_3)
Calcium	83.68	40
Carbon	6.42	12
Oxygen	9.91	48

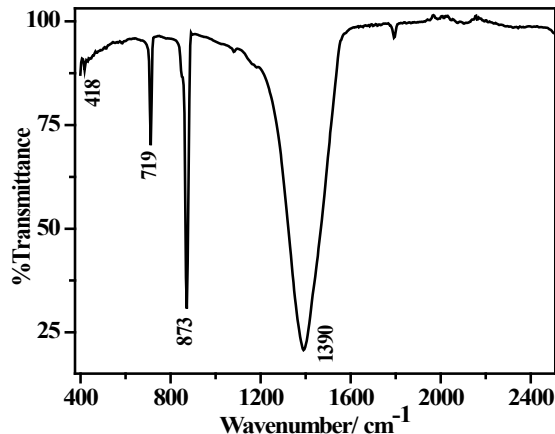


Figure 4: FT-IR spectrum of CaCO_3 NPs.

Optical absorption

The UV-Visible absorption spectroscopy is an efficient technique to monitor the optical properties of nanoparticles. CaCO_3 NPs solution used to establish the absorption spectrum, which was prepared by dissolving the nanoparticles in distilled water and sonicated for about 1 h. As can be seen in the Figure 5, broad absorption maxima corresponding to CaCO_3 NPs appeared at 272 and 325 nm.

Electrochemical impedance studies

In $[\text{K}_4\text{Fe}(\text{CN})_6]^{-3/4}$ solution containing 0.1M KCl, surface phenomenon and charge transfer resistance of BCPE and CaCO_3 NPs MCPE was studied (Figure 6) by EIS technique with frequencies swept from 10^4 to 0.01 Hz. Semicircle portion was observed at higher frequencies corresponded to the electron transfer limiting process. On CaCO_3 NPs MCPE, lower R_{ct} value ($2289\ \Omega$) was observed as compared with BCPE ($4585\ \Omega$) which is due to presence of CaCO_3 NPs on the electrode surface could improve the conductivity of CPE and facilitated the electron transfer between solution and electrode interface.

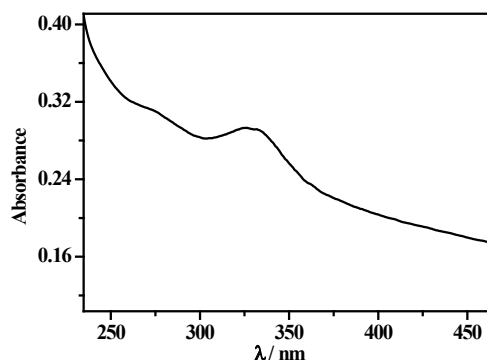


Figure 5: Absorption spectrum of CaCO₃ NPs (concentration=0.5 mM, path length=1.0 cm).

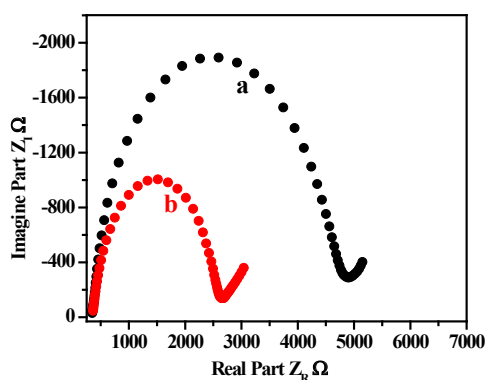
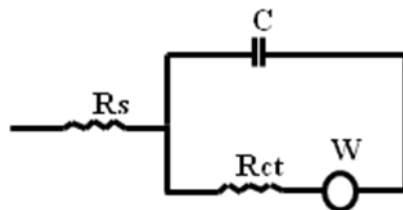


Figure 6: Nyquist diagrams of (curve a) BCPE and (curve b) CaCO₃ NPs MCPE in 5 mM [Fe(CN)₆]^{3-/4-} (1:1) containing 0.1M KCl. Inset: Randles model to fit the EIS.



Electrocatalytic oxidation of FsDNA

Figure 7 shows the DPV's of 300 μg ml⁻¹ FsDNA in pH 7 on the surface of BCPE and CaCO₃ NPs MCPE. Two distinct anodic peaks were observed at potential of 0.734 V and 1.047 V where as anodic peaks were observed at 0.720 V and 1.028V for CaCO₃ NPs MCPE. These two anodic peaks were due to electrochemical oxidation of guanine and adenine residues in FsDNA respectively.

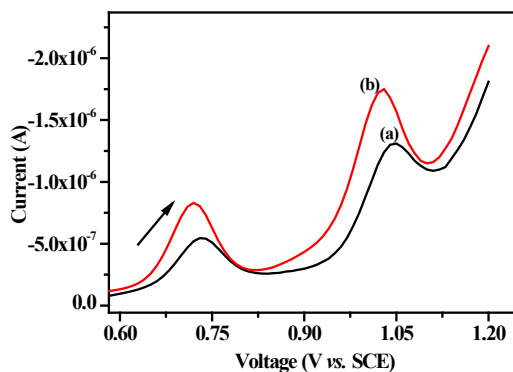


Figure 7: DPV's of 300 μg mL⁻¹ FsDNA on BCPE (curve a) and CaCO₃ NPs MCPE (curve b) in 0.1M PBS of pH 7.0.

The observed values of guanine and adenine residues in FSDNA further confirmed by simultaneous addition of adenine and guanine at CaCO_3 NPs MCPE and by individual addition of adenine and guanine as shown in the Figure 8 (a) and (b). Compared to the BCPE, the CaCO_3 NPs MCPE showed the significant reduction in the peak potential and remarkable enhancement of peak current. This proved that, the electro-catalytic activity of CaCO_3 NPs MCPE in oxidation of FSDNA.

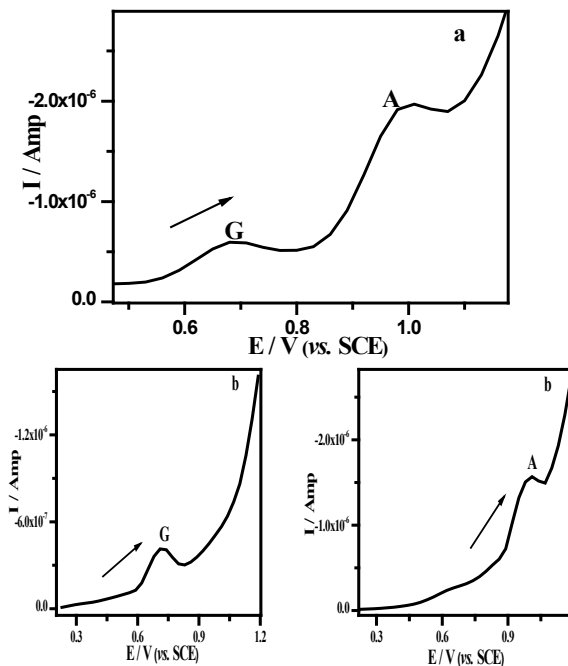


Figure 8: (a) Simultaneous and (b) individual DPV's of 10 μM guanine (G) and 10 μM adenine (A) on CaCO_3 NPs MCPE in 0.1M PBS of pH 7.0.

CV's of 300 $\mu\text{g ml}^{-1}$ FSDNA in pH 7.0PBS on modified and bare electrode has shown in Figure 9. Well-defined two oxidation peaks observed at 0.772 V and 1.067 V for BCPE, where as for CaCO_3 NPs MCPE, oxidation peaks observed at 0.751 V and 1.046 V. The resulted observation is due to diffusion process at electrically charged electrode surface [29].

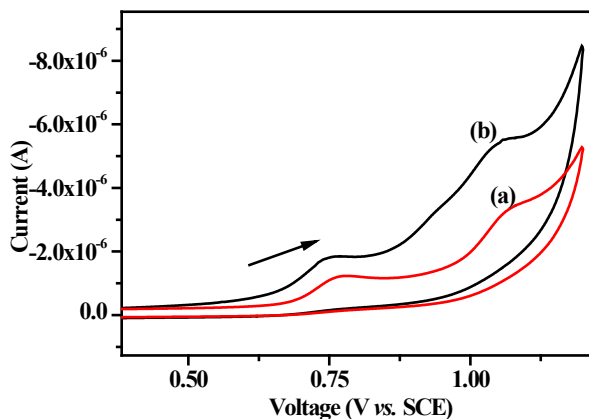
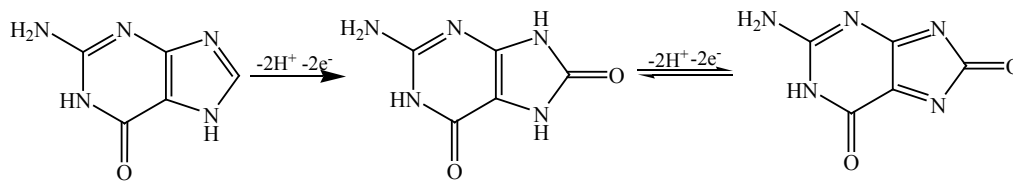
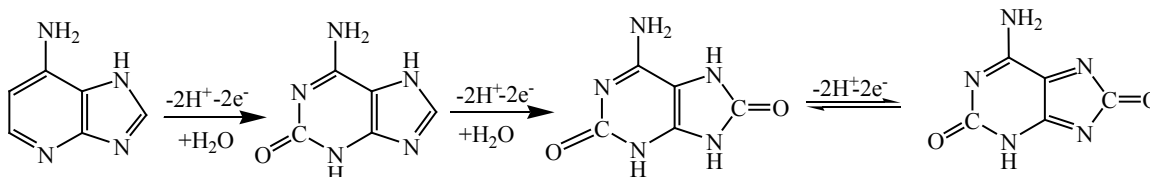


Figure 9: CV's of 300 $\mu\text{g mL}^{-1}$ FSDNA on BCPE (curve a) and CaCO_3 NPs MCPE (curve b) in 0.1M PBS of pH 7.0 at 0.05 Vs^{-1} .

In case of CaCO_3 NPs MCPE, on comparison with BCPE, shift in peak potentials along with increase in peak currents. This result reveals that, a remarkable catalytic activity of CaCO_3 NPs MCPE towards the electrochemical oxidation of adenine and guanine residues of FSDNA. Arvand et al. reported that the total loss of four electrons and six electrons corresponds to guanine and adenine in two and three step respectively and the first step involves two electrons and two proton transfer process [14]. The possible mechanism is depicted in scheme 1.



Guanine



Adenine

Scheme 1: Possible oxidation mechanism of guanine and adenine.

Effect of concentration

The simultaneous (Figure 10) and individual (Figures 11a and b) determination of G and A were studied in pH 7 PBS. With increase in concentration of each base, the peak current increased linearly in the range of 2 to 40 μM for G and 0 to 40 μM for A, whereas the peak potential remains unaffected. Two well distinguished oxidation peaks were observed for simultaneous determination, confirmed that there is no much interfering with each other. Further, compared to other sensors applied for detection of adenine and guanine or DNA, offered method showed more advantages such as more simplicity, low cost and ease of preparation.

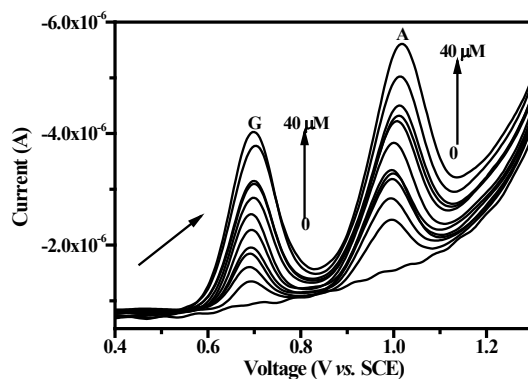


Figure 10: Simultaneous DPV's of guanine (0 μM to 40 μM) and adenine (0 μM to 40 μM) on CaCO_3 NPs MCPE.

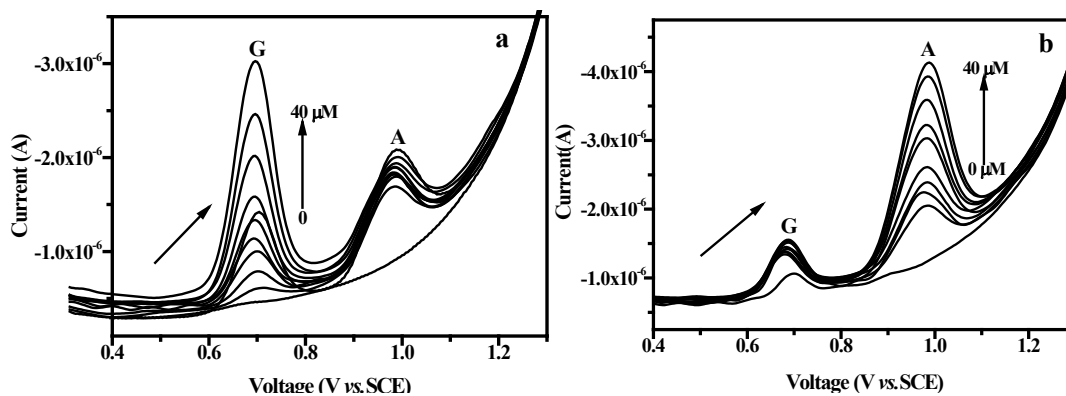


Figure 11: Individual DPV's of (a) guanine (0 μM to 40 μM) in presence of 10 μM adenine and (b) adenine (0 μM to 40 μM) in presence of 10 μM guanine on CaCO_3 NPs MCPE.

CONCLUSION

CaCO₃ NPs prepared by using bubbling method. The synthesized nanoparticles used to construct the carbon paste electrode that showed good electrocatalytic response towards FsdNA. Oxidation peak potential of adenine and guanine matches with the FsdNA and enhancement in peak current, due to the high surface area on the working electrode.

ACKNOWLEDGEMENT

The authors, gratefully acknowledges the financial support received from VISION GROUP ON SCIENCE AND TECHNOLOGY (VGST), Government of Karnataka, India and Kanasparsha Chemicals Pvt. Ltd, Bengaluru for technical support.

REFERENCES

- [1] Dinamani, M., Vishnu Kamath, P., and Sheshadri, R., *Mater. Res. Bull.*, **2002**. 37: p. 661.
- [2] Spanos, N., and Koutsoukos, P. G., *J. Phys. Chem. B.*, **1998**. 102: p. 6679.
- [3] Chen, J., and Xiang, L., *Powder Technol.*, **2009**. 189: p. 64.
- [4] Islam, K. N., et al., *Power Technol.*, **2011**. 213: p. 188.
- [5] Guo, F., et al., *Mater. Lett.*, **2007**. 61: p. 4937.
- [6] Wang, C., et al., *Powder Technol.*, **2006**. 163: p. 134.
- [7] Nancollas, G. H., Kazmierczak, T. F., and Schuttringer, E., *Corrosion*, **1981**. 37: p. 76.
- [8] Nurul Islam, K., et al., *J. Nanomater*, **2012**. 201: p. 21.
- [9] Gorna, K., et al., *Mater. Sci. Eng A.*, **2008**. 477: p. 217.
- [10] Chan, D. S. H., et al., *Chem. Commun.*, **2009**. 45: pp: 7479-7481.
- [11] Ma, B. Y. H., et al., *Chem. Commun*, **2010**. 46: pp: 8534-8536.
- [12] Ma, D. L., et al., *Nucleic acid Res*, **2011**. 39: p. 67.
- [13] Motaghed, M. R., and Arvand, M., *J. Chem. Sci.*, **2014**. 126: p. 1031.
- [14] Arvand, M., Motaghed, R., and Niazi, A., *Electrochimica acta*, **2013**. 89: pp: 669-679.
- [15] Xiao, F., et al., *Electrochimica acta*, **2008**. 53: p. 7781.
- [16] Wang, J., *Anal. Chem.*, **1999**. 71: p. 328.
- [17] Palecek, E., *Bioelectroch. Bioener.*, **1986**. 15: p. 275.
- [18] Palecek, E., Kolar, V., and Jelen, F., *Bioelectroch. Bioener.*, **1990**. 23: p. 285.
- [19] Palecek, E., et al., *Anal. Chim. Acta.*, **1993**. 272: p. 175.
- [20] Jelen, E., Tomschik, M., and Palecek, E., *J. Electroanal. Chem.*, **1997**. 423: p. 141.
- [21] Ontko, A. C., et al., *Inorg. Chem.*, **1999**. 38: p. 1842.
- [22] Abbaspour, A., and Ghaffarinejad, A., *Electrochim. Acta.*, **2010**. 55: p. 1090.
- [23] Tu, X., et al., *Microchem. Acta.*, **2010**. 169: p. 33.
- [24] Sun, W., et al., *Biosens. Bioelectron.* **2008**. 24: p. 988.
- [25] Shahrokhian, S., et al., *Bioelectrochem.*, **2012**. 86: p. 78.
- [26] Sun, W., et al., *Electrochem. Commun.*, **2008**. 10: p. 298.
- [27] Hariharan, M., et al., *Inter. J. Sci. Res. Pub.*, **2014**. 4: p. 1.
- [28] Yellappa, S., et al., *Inter. J. Chem.* **2015**. 36: p. 1736.
- [29] Yellappa, S., et al., *Bioconjugate Chem.*, **2006**. 17: p. 1418.